

## Comparison with statistical analysis of signal correction in diffusion weighted MR image

**Poster No.:** C-0291  
**Congress:** ECR 2016  
**Type:** Scientific Exhibit  
**Authors:** Y. Konishi<sup>1</sup>, Y. Kanazawa<sup>1</sup>, T. Usuda<sup>1</sup>, Y. Matsumoto<sup>1</sup>, H. Hayashi<sup>1</sup>, M. Matsuda<sup>2</sup>, M. Harada<sup>1</sup>; <sup>1</sup>Tokushima/JP, <sup>2</sup>Tokyo/JP  
**Keywords:** MR physics, MR, MR-Diffusion/Perfusion, Physics, Statistics, Technical aspects, Image verification, Quality assurance

Any information contained in this pdf file is automatically generated from digital material submitted to EPOS by third parties in the form of scientific presentations. References to any names, marks, products, or services of third parties or hypertext links to third-party sites or information are provided solely as a convenience to you and do not in any way constitute or imply ECR's endorsement, sponsorship or recommendation of the third party, information, product or service. ECR is not responsible for the content of these pages and does not make any representations regarding the content or accuracy of material in this file.

As per copyright regulations, any unauthorised use of the material or parts thereof as well as commercial reproduction or multiple distribution by any traditional or electronically based reproduction/publication method is strictly prohibited.

You agree to defend, indemnify, and hold ECR harmless from and against any and all claims, damages, costs, and expenses, including attorneys' fees, arising from or related to your use of these pages.

Please note: Links to movies, ppt slideshows and any other multimedia files are not available in the pdf version of presentations.

[www.myESR.org](http://www.myESR.org)

## Aims and objectives

Diffusion weighted (Dw) magnetic resonance (MR) imaging has recently become a useful technique for evaluating various diseases, e.g., acute cerebral infarctions and tumors [1]. Dw MR imaging is a method for imaging of incoherent motions. In Dw MR imaging, the  $b$ -values represents the intensity of the gradient magnetic field. Dw images with high  $b$ -values are influenced less by perfusion but more by diffusion. It is becoming more important to apply an analysis method with high  $b$ -values, e.g., q-space -analyzed Dw MRI [2], diffusional kurtosis imaging [3], and modified tri-exponential analysis of intravoxel incoherent motion [4]. The signal intensity (SI) of the Dw image decreases by echo time (TE) prolongation, and this leads to a low signal-to-noise ratio (SNR) [5]. Additionally, it has been reported that a low SNR influences the determination of the apparent diffusion coefficients (ADC) [6], or leads to failure in measuring diffusion anisotropy [7].

MR images are commonly presented as magnitude images. The magnitude images are made by reconstruction of real images and imaginary images [8]. These images are acquired by a quadrature detector system; they are influenced by the statistical image noise. Before reconstruction, the noise from these images has characteristics of a Gaussian distribution. On the other hand, the magnitude image has not only the characteristics of a Gaussian distribution, but also of a Rician distribution [9]. They indicate that the magnitude image does not have a negative value. This distribution has characteristics that differ from those of the Gaussian distribution. Many reports applied to the Rician distribution, e.g.,  $R_2^*$  estimation of the liver [10], and determination of the optimal  $b$ -value in diffusion tensor imaging [11]. Thus, it is important for MR imaging to assess the relationship between the signal values and the Rician distribution.

Therefore, the signal correction in high- $b$ -value images is expected to yield improved images as a consequence of application of the Rician distribution. We became interested in correction schemes from past reports. Previous articles did not describe high- $b$ -value Dw signals corrected with use of these schemes. Our purpose in this our study was to correct the noise in order to improve the SNR of Dw images with high  $b$ -value by using two correction schemes based on the probability distributions.

## Methods and materials

### 1 Magnitude image of MR imaging

MR images consist of reconstruction of real images and imaginary images. The SI from the  $j$ th pixel in a complex MR image was described by Henkelman [4]:

$$S_j = A_j + N_{Rj} + iN_{Ij} \quad (1)$$

**Fig. 1**

**References:** Tokushima University - Tokushima/JP

where  $S_j$  is the measured signal amplitude,  $A_j$  is the true signal amplitude of the  $j$ th pixel, and  $N_{Rj}$  and  $N_{Ij}$  are the noise components. The magnitude of the SI,  $M_j$ , is described as follows:

$$M_j = |S_j| = [(A_j + N_{Rj})^2 + N_{Ij}^2]^{1/2} \quad (2)$$

**Fig. 2**

**References:** Tokushima University - Tokushima/JP

## 2 Probability distribution

The probability density function (PDF) for the Gaussian distribution for the measured pixel intensity  $M$  is given by

$$P_M(M) = \frac{1}{\sqrt{2\pi\sigma^2}} \exp\left(-\frac{(M-\mu)^2}{2\sigma^2}\right) \quad (3)$$

**Fig. 3**

**References:** Tokushima University - Tokushima/JP

where  $\mu$  is mean, and  $\sigma$  is the standard deviation (S.D.). This probability density distribution show in Fig. 4.

# Gaussian distribution

$$P_M(M) = \frac{1}{\sqrt{2\pi\sigma^2}} \exp\left(-\frac{(M - \mu)^2}{2\sigma^2}\right)$$

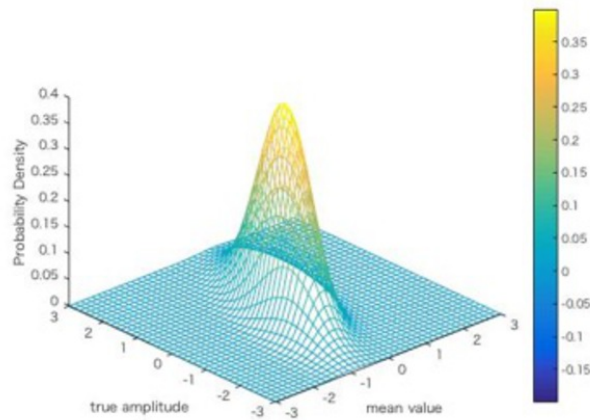


**Fig. 4:** The probability density distribution of the Gaussian distribution for  $M$ .

**References:** Tokushima University - Tokushima/JP

The PDF for the Rician distribution for  $M$  is given in reference [4]:

$$P_M(M) = \frac{M}{\sigma^2} \exp\left(-\frac{(M^2 + A^2)}{2\sigma^2}\right) I_0\left(\frac{A \cdot M}{\sigma^2}\right) \quad (4)$$

**Fig. 5**

**References:** Tokushima University - Tokushima/JP

where  $A$  is the true pixel intensity, and  $I_0$  is the modified zeroth order Bessel function. Besides, this probability density distribution show in Fig.6.

# Rician distribution

$$P_M(M) = \frac{M}{\sigma^2} \exp\left(-\frac{(M^2 + A^2)}{2\sigma^2}\right) I_0\left(\frac{A \cdot M}{\sigma^2}\right)$$

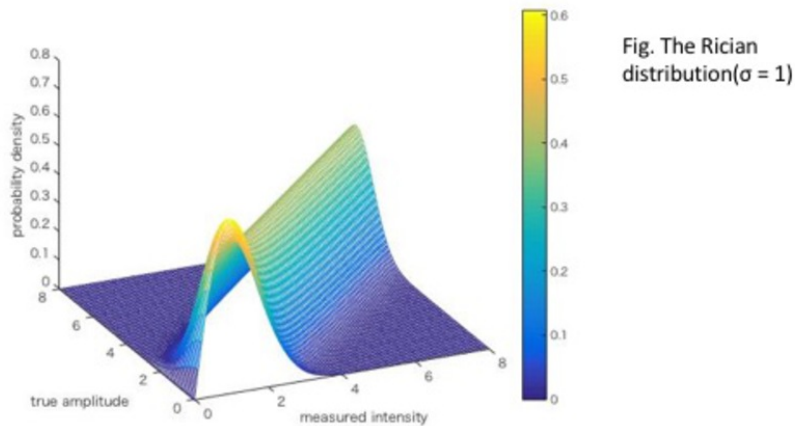


**Fig. 6:** The probability density distribution of the Rician distribution for M. Standard deviation # is 1.

**References:** Tokushima University - Tokushima/JP

The characteristics of the Rician distribution differ from those of the Gaussian distribution when the SNR is low. However, when the SNR is high, it is approximately equal to the Gaussian distribution [9]. When the SNR is high, the Rician distribution is approximated by Eq. (5) [9]:

$$P_M(M) \approx \frac{1}{\sqrt{2\pi\sigma^2}} \exp\left(-\frac{(M - \sqrt{A^2 + \sigma^2})^2}{2\sigma^2}\right) \quad (5)$$

**Fig. 7**

**References:** Tokushima University - Tokushima/JP

The noise distribution of a magnitude image at a high SNR can be regarded as the Gaussian distribution with mean  $\#(A^2 + \#^2)$  and variance # as determined by this equation.

The postprocessing correction scheme introduced by Gudbjartson and Patz suggested that it was possible to reduce noise by using the following relationship [9]:

$$\tilde{A}_1 = \sqrt{|M^2 - \sigma^2|} \quad (6)$$

**Fig. 8**

**References:** Tokushima University - Tokushima/JP

where  $\tilde{A}_1$  is corrected SI. We used Eq. (6) as behaving the correction scheme based on the Rician distribution.

There is a relationship,  $M^2 = A^2 + 2\sigma^2$ , between the mean of the measured SI and the true SI in the magnitude image [4]. Then, the following correction scheme has been established [9]:

$$\tilde{A}_2 = \sqrt{|M^2 - 2\sigma^2|} \quad (7)$$

**Fig. 9**

**References:** Tokushima University - Tokushima/JP

where  $\tilde{A}_2$  is the corrected SI. We established Eq. (7) as behaving the correction scheme based on the Gaussian distribution.

### 3 MR imaging

On a 1.5T MRI system (Signa HDxt, GE Healthcare, Waukesha, WI, USA), Dw imaging of a phantom was performed with single-shot spin-echo echo-planner imaging (SS-SE-EPI). To acquire Dw images of ADC, we made phantoms by using sucrose solutions of different concentrations (10, 30, and 50 wt%) [12]. SI decay model show in Fig. 10.

# Sucrose phantom

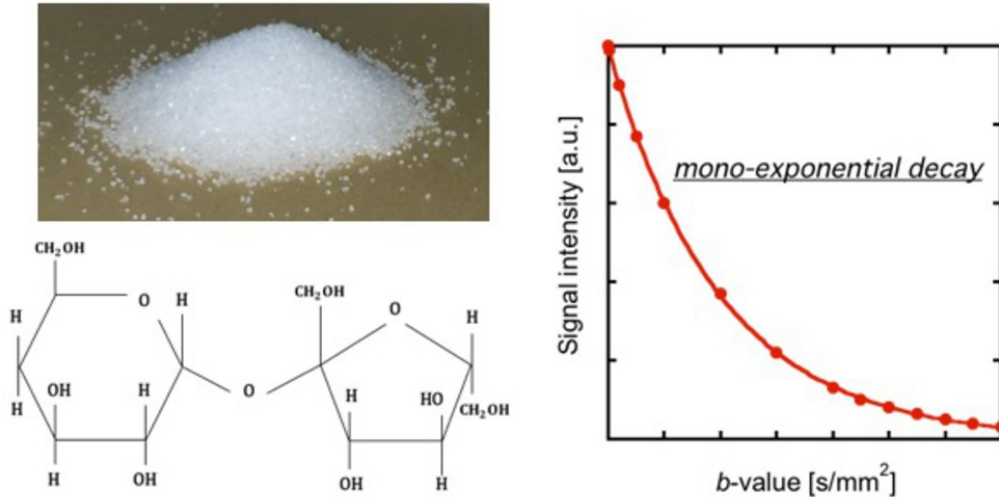


**Fig. 10:** Signal intensity decay model in sucrose phantom. The signal intensity of this phantom follow mono-exponential decay model.

**References:** Tokushima University - Tokushima/JP

Each phantom was placed in the center of a standard head coil. The other imaging parameters show Table 1.

Parameters	Setting values
Sequences	Single shot spin-echo EPI
b-values [s/mm <sup>2</sup> ]	0, 20, 200, 500, 1000, 2000, 3000, 4000, 4500, 5000, 5500, 6000, 6500, and 7000.
TR/TE [ms]	5000/129
FOV [cm <sup>2</sup> ]	12.8 × 6.4
Slice thickness [mm]	10
Band width [Hz/pixel]	166.7

**Table 1:** Imaging parameters.

**References:** Tokushima University - Tokushima/JP

#### 4 Data analysis

A typical example of the region-of-interest (ROI) setting is shown in Fig. 1. We measured SIs at the ROI (for the size for 15 × 15 pixels). Then we measured the mean SI  $M$  and S.D.  $\#$  in the ROI. Next, we calculated each PDF by using an in-house program from MATLAB (MathWorks, Natick, MA, USA). We derived the median value  $A$  from each PDF, i.e., we regarded  $A$  as the true SI. Furthermore, we calculated each corrected SI ( $\tilde{A}_1$  and  $\tilde{A}_2$ ) from each Eq. (6) and Eq. (7).

To assess the results of correcting the measured SI in Dw imaging, we evaluated error values in each  $b$ -value Dw image. The error value is defined by Eq. (8):

$$error [\%] = \frac{|A - \tilde{A}|}{A} \times 100 \quad (8)$$

#### Fig. 11

**References:** Tokushima University - Tokushima/JP When the error was small, we regarded the effect as accurate performance.

The chart of this experiment shows in Fig. 12.



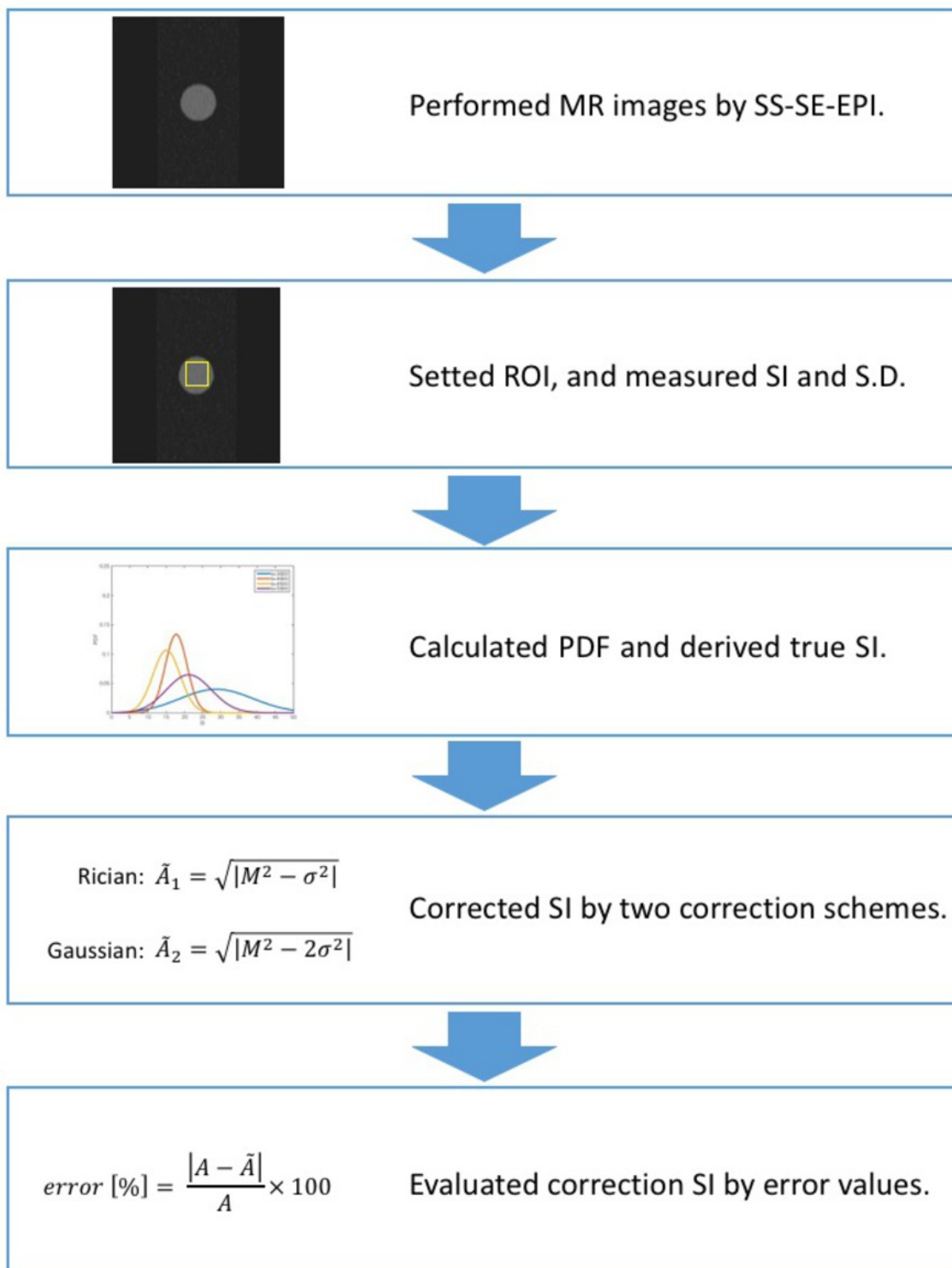


**Fig. 12:** Chart of this experiments.

**References:** Tokushima University - Tokushima/JP

Images for this section:

# Gaussian distribution

$$P_M(M) = \frac{1}{\sqrt{2\pi\sigma^2}} \exp\left(-\frac{(M - \mu)^2}{2\sigma^2}\right)$$

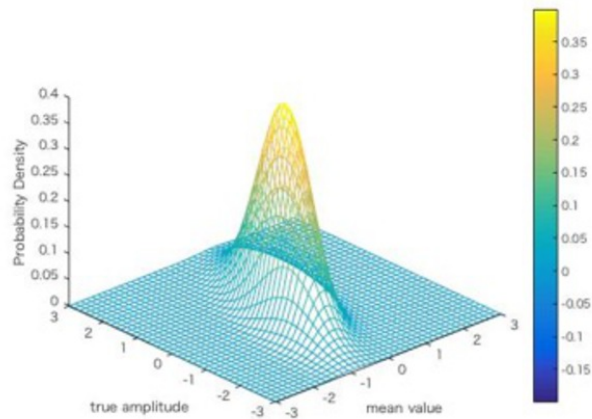


**Fig. 4:** The probability density distribution of the Gaussian distribution for M.

© Tokushima University - Tokushima/JP

# Rician distribution

$$P_M(M) = \frac{M}{\sigma^2} \exp\left(-\frac{(M^2 + A^2)}{2\sigma^2}\right) I_0\left(\frac{A \cdot M}{\sigma^2}\right)$$

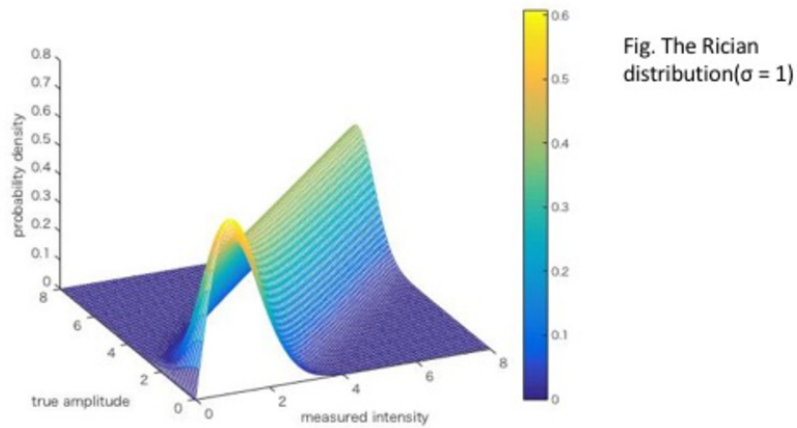


**Fig. 6:** The probability density distribution of the Rician distribution for M. Standard deviation # is 1.

© Tokushima University - Tokushima/JP

# Sucrose phantom

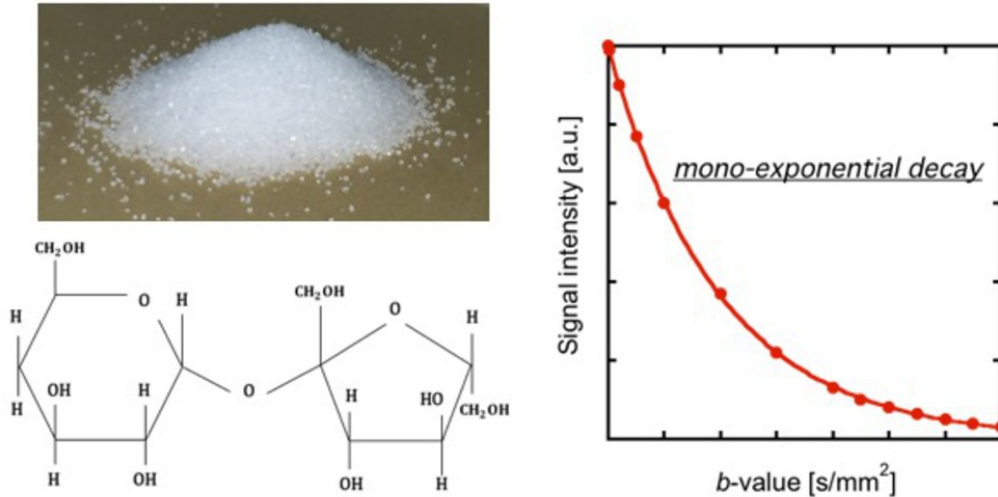


**Fig. 10:** Signal intensity decay model in sucrose phantom. The signal intensity of this phantom follow mono-exponential decay model.

© Tokushima University - Tokushima/JP

Parameters	Setting values
Sequences	Single shot spin-echo EPI
b-values [s/mm <sup>2</sup> ]	0, 20, 200, 500, 1000, 2000, 3000, 4000, 4500, 5000, 5500, 6000, 6500, and 7000.
TR/TE [ms]	5000/129
FOV [cm <sup>2</sup> ]	12.8 × 6.4
Slice thickness [mm]	10
Band width [Hz/pixel]	166.7

**Table 1:** Imaging parameters.

© Tokushima University - Tokushima/JP

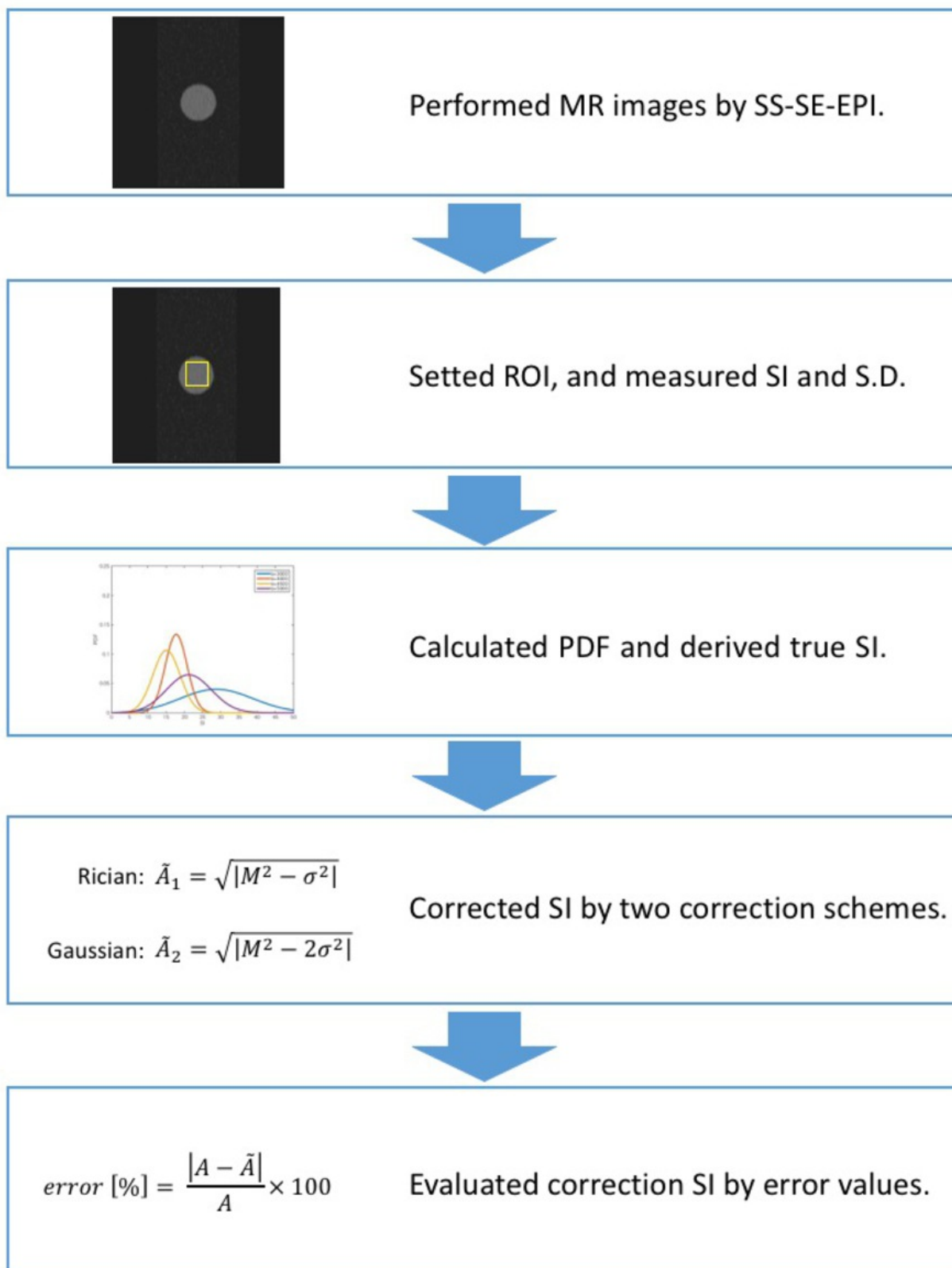




**Fig. 12:** Chart of this experiments.



## Results

Table 2 shows the relationship between  $b$ -values and several signal-to-standard deviation ratios for each phantom.

$b$ -value [s/mm <sup>2</sup> ]	$A/\sigma$		
	10 [wt%]	30 [wt%]	50 [wt%]
0	51.5	58.0	87.5
20	94.4	79.0	139.4
200	76.7	82.6	100.9
500	60.2	73.1	87.7
1000	34.1	48.8	94.6
2000	8.1	14.0	34.5
3000	2.6	8.8	15.4
4000	3.8	2.6	16.7
4500	6.2	5.8	17.5
5000	3.0	3.7	5.0
5500	1.4	3.2	5.8
6000	2.4	2.8	3.8
6500	2.4	1.9	5.0
7000	2.6	2.4	5.0

 : Error value  $\geq$  5% (correction scheme based on Gaussian distribution)  
 : Error value  $\geq$  5% (correction scheme based on Rician distribution)

**Table 2:** Relationship between  $b$ -values and several signal-to-standard deviation ratios.

**References:** Tokushima University - Tokushima/JP

Figure 13 shows the Dw images (a, b, and c) and the PDFs from the Rician distribution (d, e, and f). Each SI for a Dw image was shown to decrease at the higher  $b$ -values. The PDFs shifted to low intensity, and the variances were low at higher  $b$ -values.



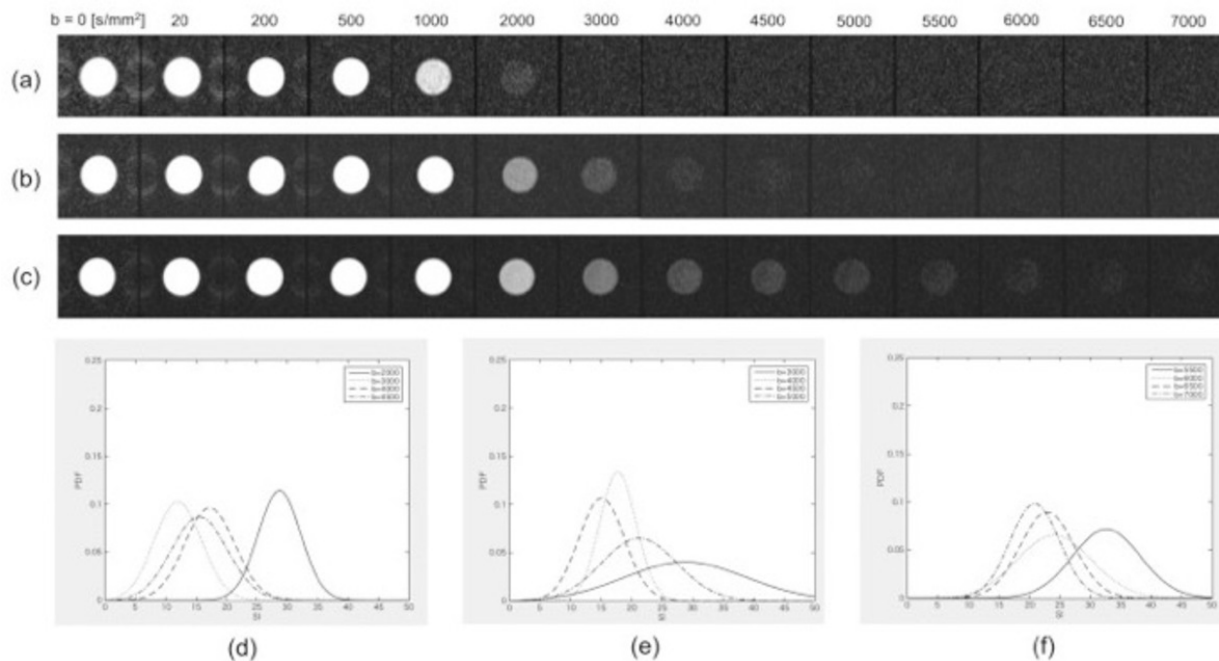


**Fig. 13:** Diffusion weighted images and probability distribution function from the Rician distribution.

**References:** Tokushima University - Tokushima/JP

Figure 14 shows the error between the correction SI and the true SI. The highest error values for each phantom concentration (10, 30, and 50 wt%), in correction by the correction scheme based on the Rician distribution, were 7.3, 2.4, and 0.1 [%], respectively. The highest error values for each of the three phantom concentration in correction by the correction scheme based on the Gaussian distribution, were 20.3, 11.6, and 3.4 [%], respectively. When  $A/\#$  was lower than 1.4, the error value was determined by application of the correction scheme based on the Rician distribution, which was higher than 5.0 [%]. In addition, when  $A/\#$  was lower than 3.0, the error values were determined by application of the correction scheme based on the Gaussian distribution, which were higher than 5.0 [%] (Table 2 and Fig.14).

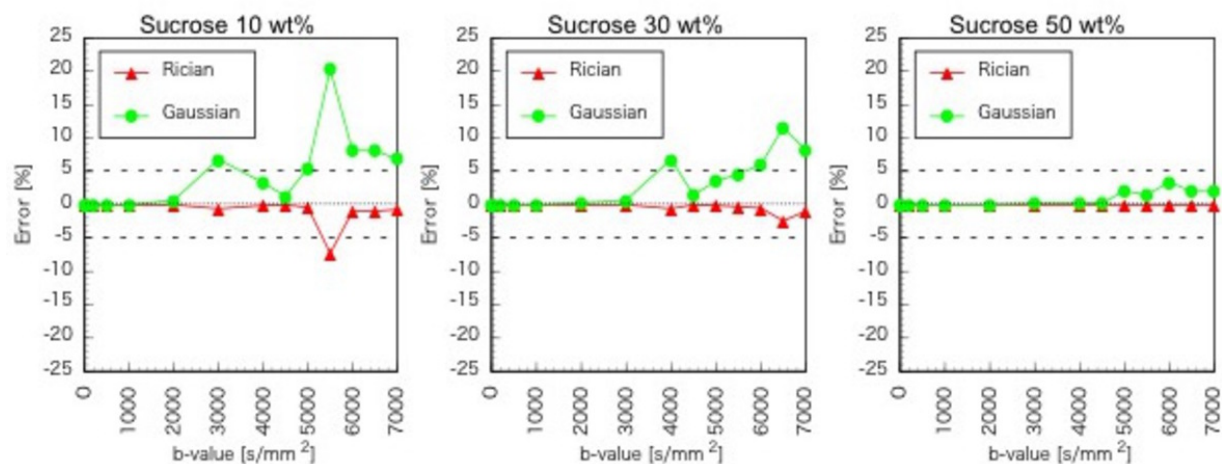


**Fig. 14:** Error value between the correction signal intensity and true signal intensity.  
**References:** Tokushima University - Tokushima/JP

Images for this section:

$b$ -value [s/mm <sup>2</sup> ]	$A/\sigma$		
	10 [wt%]	30 [wt%]	50 [wt%]
0	51.5	58.0	87.5
20	94.4	79.0	139.4
200	76.7	82.6	100.9
500	60.2	73.1	87.7
1000	34.1	48.8	94.6
2000	8.1	14.0	34.5
3000	2.6	8.8	15.4
4000	3.8	2.6	16.7
4500	6.2	5.8	17.5
5000	3.0	3.7	5.0
5500	1.4	3.2	5.8
6000	2.4	2.8	3.8
6500	2.4	1.9	5.0
7000	2.6	2.4	5.0

: Error value  $\geq 5\%$  (correction scheme based on Gaussian distribution)

: Error value  $\geq 5\%$  (correction scheme based on Rician distribution)

**Table 2:** Relationship between  $b$ -values and several signal-to-standard deviation ratios.

© Tokushima University - Tokushima/JP

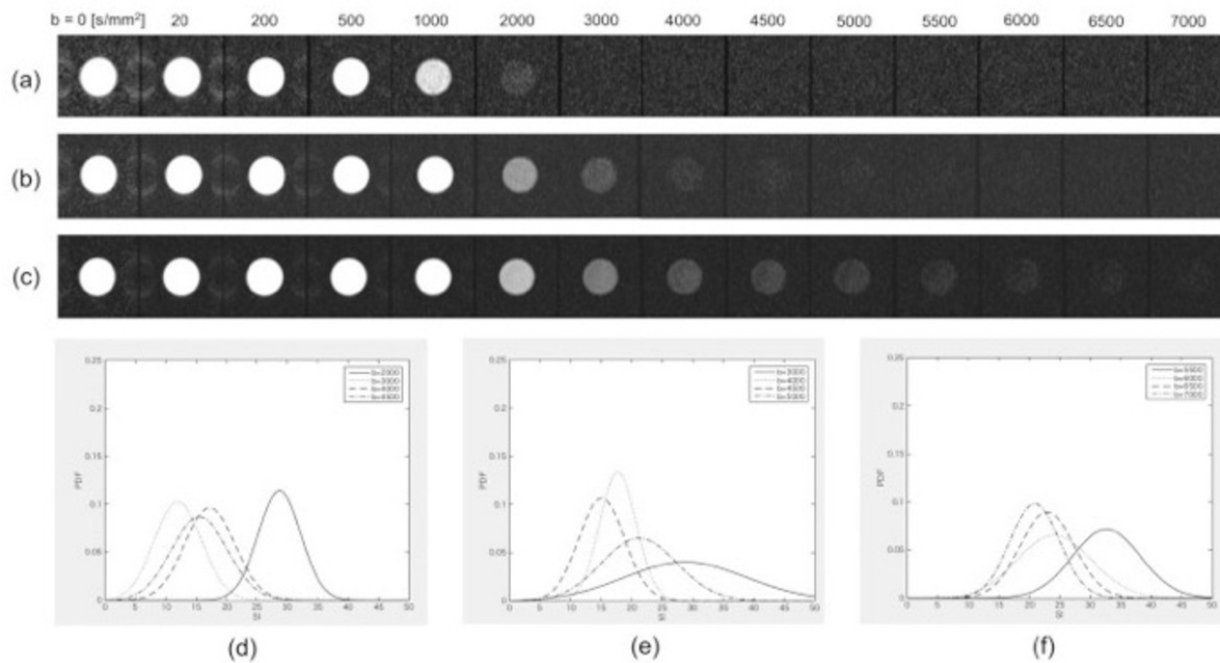


**Fig. 13:** Diffusion weighted images and probability distribution function from the Rician distribution.

© Tokushima University - Tokushima/JP

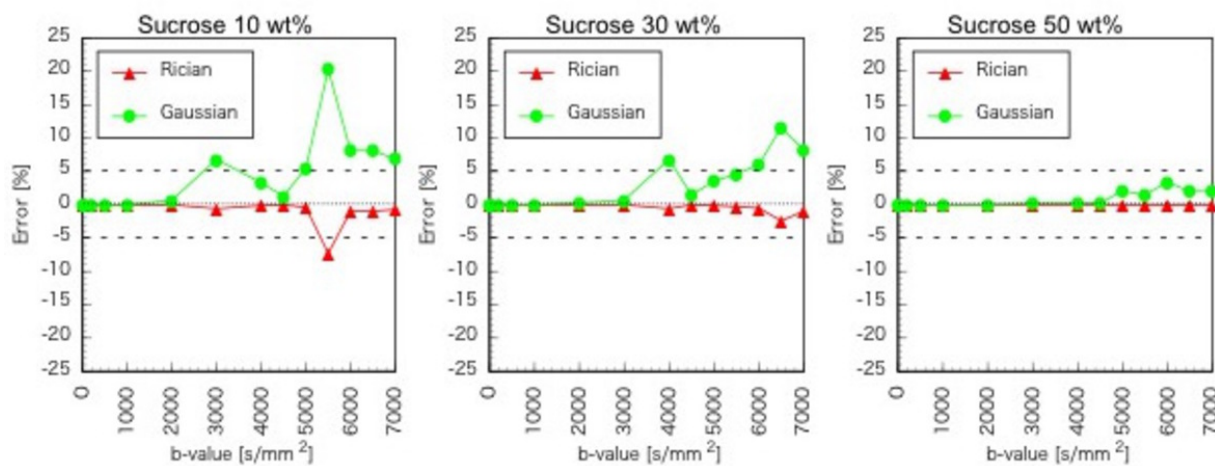


**Fig. 14:** Error value between the correction signal intensity and true signal intensity.

© Tokushima University - Tokushima/JP

## Conclusion

In Dw imaging, the correction of the SI makes it possible to apply a correction scheme based on the Rician distribution.

## Personal information

### Author Names:

Yuto Konishi<sup>1</sup>, Yuki Kanazawa<sup>2</sup>, Takatoshi Usuda<sup>1</sup>, Yuki Matsumoto<sup>1</sup>, Hiroaki Hayashi<sup>1</sup>, Tsuyoshi Matsuda<sup>3</sup>, and Masafumi Harada<sup>4</sup>

### Author Affiliations:

<sup>1</sup> School of Health Sciences, Tokushima University

<sup>2</sup> Institute of Biomedical Sciences, Tokushima University Graduate School

<sup>3</sup> MR Applications and Workflow Asia Pacific GE Healthcare Japan Corporation

<sup>4</sup> Department of Radiology and Radiation Oncology, Institute of Biomedical Sciences, Tokushima University Graduate School

### Corresponding Author and Reprint Info:

Yuki Kanazawa, PhD

Institute of Biomedical Sciences, Tokushima University Graduate School

3-18-15, Kuramoto-Cho, Tokushima City, Tokushima, 770-8509, Japan

E-mail: [yk@tokushima-u.ac.jp](mailto:yk@tokushima-u.ac.jp)

## References

1. Le Bihan D, Breton E, Lallemand D, Grenier P, Cabanis E, Laval Jeantet M. MR Imaging of Intravoxel Incoherent Motions: application to Diffusion and Perfusion in Neurologic Disorders. *Radiology*. 1986; 161: 401-407.
2. Assaf Y, Ben-Bashat D, Chapman J, Peled S, Biton IE, et al. High  $b$ -value  $q$ -Space Analyzed Diffusion-Weighted MRI: Application to Multiple Sclerosis. *Magn Reson Med*. 2002; 47: 115-126.
3. Fieremans Els, Jensen JH, Helpert JA. White matter characterization with diffusional kurtosis imaging. *NeuroImage*. 2011; 58: 177-188.
4. Ohno N, Miyati T, Kobayashi S, Gabata T. Modified Triexponential Analysis of Intravoxel Incoherent Motion for Brain Perfusion and Diffusion. *J Magn Reson Imaging*. 2015; e-pub. doi: 10.1002/jmri.25048.
5. Gatidis S, Schmidt H, Martirosian P, Nikolaou K, Schwenzer NF#Apparent Diffusion Coefficient-Dependent Voxelwise Computed Diffusion-Weighted Imaging : An Approach for Improving SNR and Reducing  $T_2$  Shine-Through Effects. *J Magn Reson Imaging*. 2015; e-pub. doi: 10.1002/jmri.25044
6. Dietrich O, Heiland S, Sartor K. Noise Correction for the Exact Determination of Apparent Diffusion Coefficients at Low SNR. *Magn Reson Med*. 2001; 45: 448-453.
7. Bastin ME, Armitage PA, Marshall I. Atheoretical study of the effect of experimental noise on the measurement of anisotropy in diffusion imaging. *Magn Reson Imaging* 1998; 16: 773-785.
8. Henkelman RM. Measurement of signal intensities in the presence of noise MR images. *Med phys*. 1985; 12(2): 232-233.
9. Gudbjartsson H, Patz S. The Rician Distribution of Noisy MRI Data. *Magn Reson Med*.1995; 34(6): 910-914.
10. Yokoo T, Yuan Q, Senegas J, Wiethoff AJ, Pedrosa I. Quantitative  $R_2^*$  MRI of the Liver With Rician Noise Models for Evaluation of Hepatic Iron Overload : Simulation, Phantom, and Early Clinical Expertence. *J Magn Reson Imaging*. 2015; e-pub. doi: 10.1002/jmri.24948

11. Taylor PA, Biwal B. Geometric analysis of the  $b$ -dependent effects of Rician signal noise on diffusion tensor imaging estimates and determining an optimal  $b$  value. *Magn Reson Imaging*. 2011; 29: 777-788.

12. Tamura T, Usui S, Akiyama S. Investigation of a phantom for Diffusion Weighted Imaging That Contorlled the Apparent Diffusion Coefficient Using Gelatin and Sucrose. *Nihon houshasen Gijutu Gakkai Zasshi*. 2009; 65(11): 1485-1493.